Cell Reports, Volume *37*

Supplemental information

Synaptogenic activity of the axon guidance molecule Robo2 underlies hippocampal circuit function

Heike Blockus, Sebi V. Rolotti, Miklos Szoboszlay, Eugénie Peze-Heidsieck, Tiffany Ming, Anna Schroeder, Nuno Apostolo, Kristel M. Vennekens, Phinikoula S. Katsamba, Fabiana Bahna, Seetha Mannepalli, Goran Ahlsen, Barry Honig, Lawrence Shapiro, Joris de Wit, Attila Losonczy, and Franck Polleux

Supplemental Information

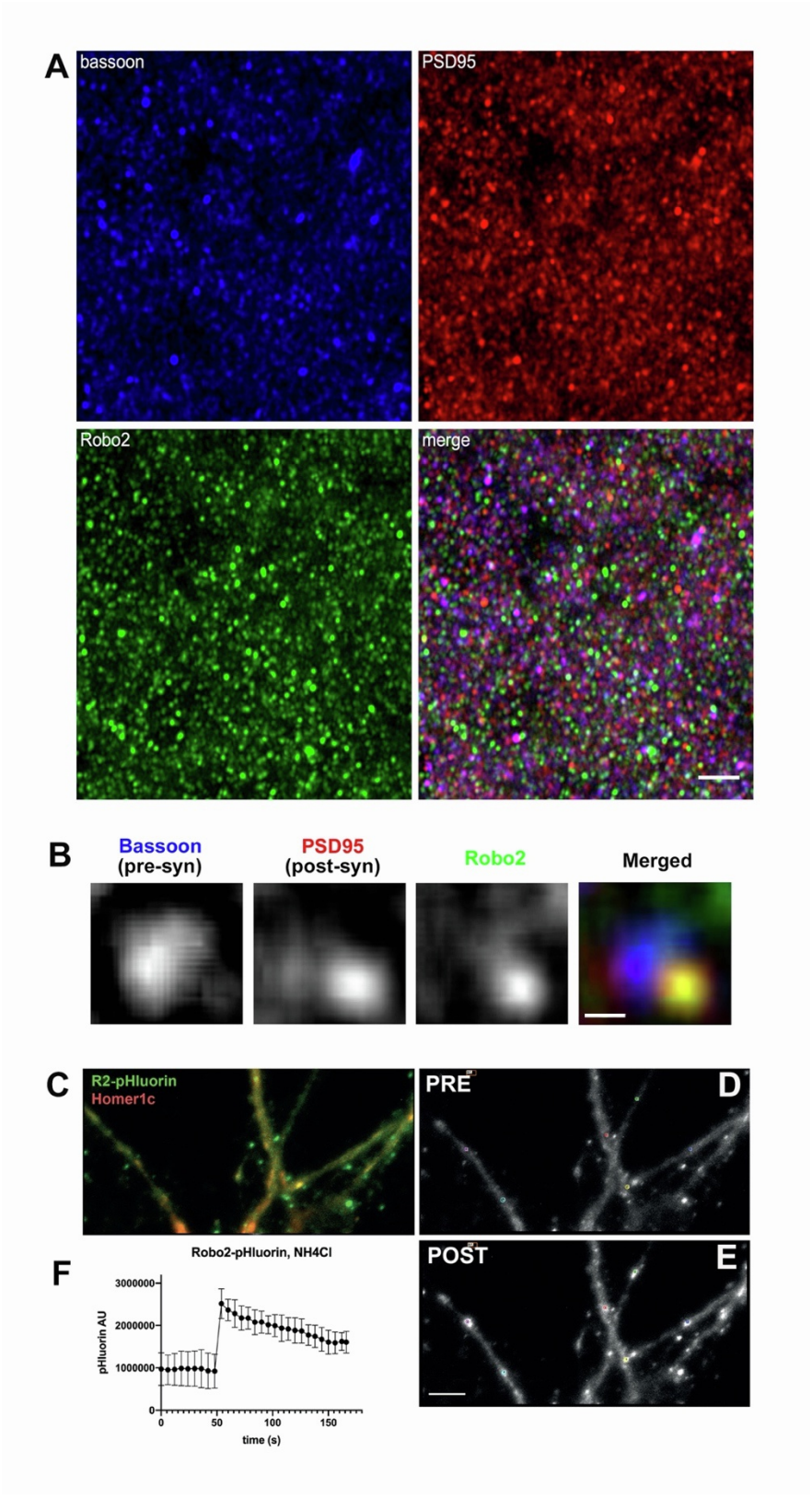

Figure S1. (related to Figure 1)

(**A**) Low magnification confocal images of immunofluorescent staining for Robo2 (green) in CA1 stratum radiatum at P35, co-stained for the presynaptic marker Bassoon (blue) and the postsynaptic marker PSD-95 (red) showing punctate staining of Robo2. Scale bar: 10μm

(**B**) High magnification of a putative synapse visualized by direct apposition of Bassoon and PSD95 shows strong enrichment of Robo2 with PSD95 suggesting postsynaptic localization. Scale bar: 2μm.

(**C-E**) Deacidification of primary dissociated cortical pyramidal neurons in culture (E15+14DIV) co-electroporated with Robo2-pHluorin and Homer1c-tdtomato with Ammonium Chloride (NH_4Cl). Scale bar: 15μm

(**F**) Quantification of green fluorescence intensity (pHluorin-Robo2) in dendritic regions of interest (ROI) shown in panels D-E before (<50sec) and after (>50sec) application of Ammonium Chloride (NH_4Cl). Increase in fluorescence after application of NH_4Cl reflects de-acidification of pHluorin-Robo2 contained in internal stores. N=3 independent experiments, at least 3 ROIs measured per experiment. Plot shows Mean with Standard deviation.

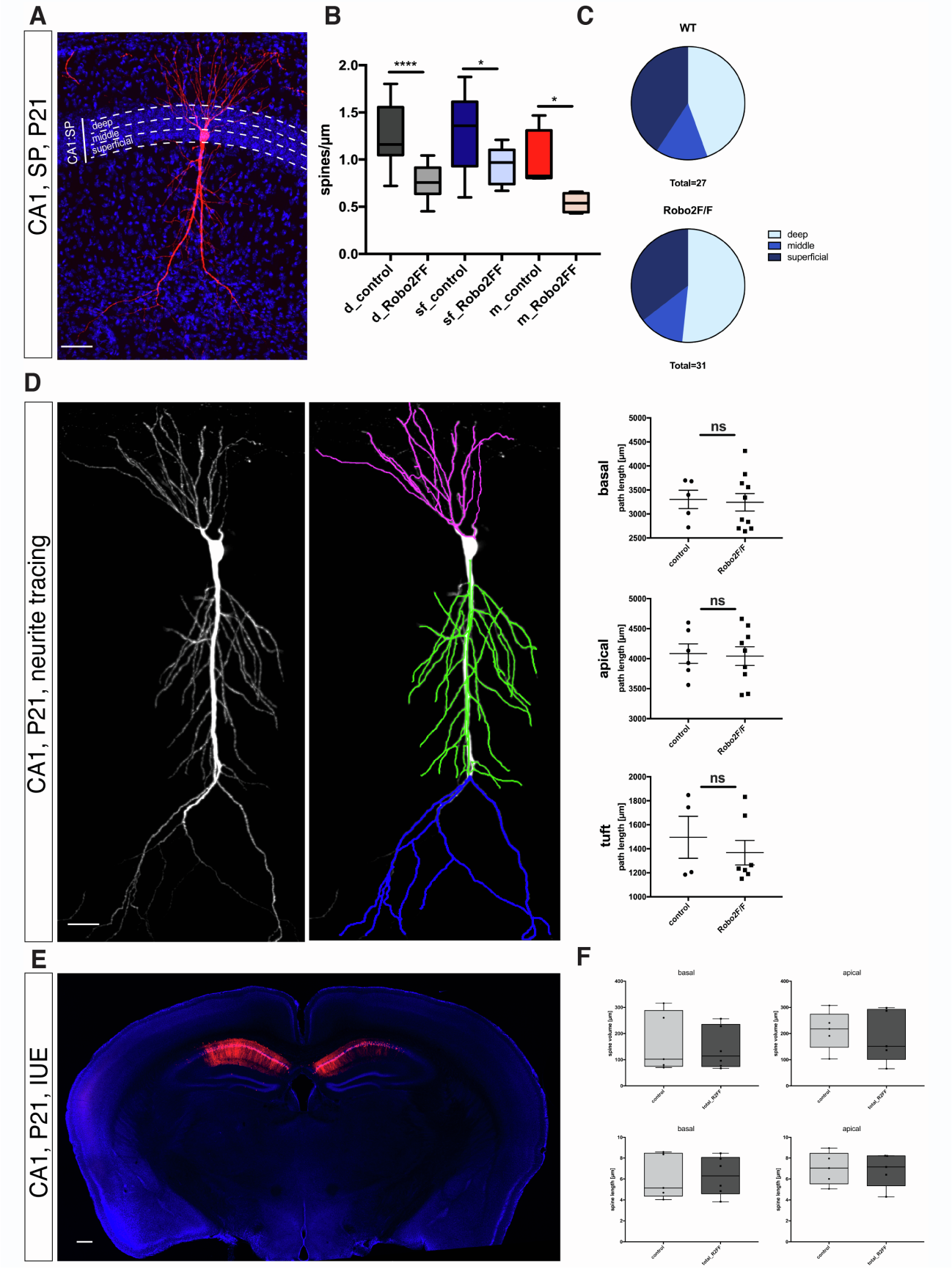
A
CA1, SP, P21
CA1:SP
deep
middle
superficial
B
spines/µm
2.0
1.5
1.0
0.5
0.0
****
*
*
d_control
d_Robo2FF
sf_control
sf_Robo2FF
m_control
m_Robo2FF
C
WT
Total=27
Robo2F/F
Total=31
deep
middle
superficial
D
CA1, P21, neurite tracing
basal
path length [µm]
ns
control
Robo2F/F
apical
path length [µm]
ns
control
Robo2F/F
tuft
path length [µm]
ns
control
Robo2F/F
E
CA1, P21, IUE
F
basal
apical
spine volume [µm]
basal
apical
spine length [µm]

17

Figure S2 (related to Figure 2).

(**A**) Binning of electroporated CA1 PNs stratum pyramidale (SP) in 3 sublayers: superficial, middle and deep. Scale bar: 40μm.

(**B**) Quantification of spine density in the SR region for control and Robo2-deleted tdTomato+ CA1 PNs over the three radial bins indicated in panel A. CA1 PNs with cell bodies located in all three SP sub-layers show statistically significant reduction of spine densities of their dendritic domains in SR. Boxplots: Median with error bars representing 95% percentile. Statistical analysis: Mann-Whitney, Group sizes (in segments) and p-values: deep: control; n=12 , $Robo2^{F/F}$**:**n=16 ($p<0.0001$)**;** middle: control: n=3 , $Robo2^{F/F}$ **:n=3 (**p= 0.0286**);** superficial: control: n=11 , $Robo2^{F/F}$ n=11 (p=0.036).

(**C**) Pie chart of soma location for CA1 PNs included in quantification shown in panels A-B.

(**D**) Robo2 is not required for total dendrite growth of CA1 PNs. Dendritic compartment-based path length analysis shows similar cumulative dendrite length between WT and Robo2 KO neurons. Neurons were reconstructed in 3D using the neurite tracer plugin in ImageJ. Scale bar: 25μm. Plots show Mean with SEM. Statistical analysis: Mann-Whitney, Group sizes (in segments) and p-values: basal: control; n=5 , $Robo2^{F/F}$**:** n=10 (p=0.59)**;** apical: control: n=6 , $Robo2^{F/F}$:n=9 (p= 0.95); tuft: control: n=4 , $Robo2^{F/F}$ n=7 (p=0.79)

(**E**) Representative low-magnification image of coronal section of electroporated hippocampus at P21 showing that the employed in utero electroporation technique effectively targets CA1, but not neighboring CA2 or CA3. Scale bar: 100μm.

(**F**) Spine volume and spine neck length are not significantly different between WT and Robo2-null CA1 PNs, indicating that no change in spine morphology is apparent in remaining spines of Robo2 KO compared to control CA1 PNs. The graph shows mean+/-SEM of spines contained in 5 segments for basal and apical dendrites.

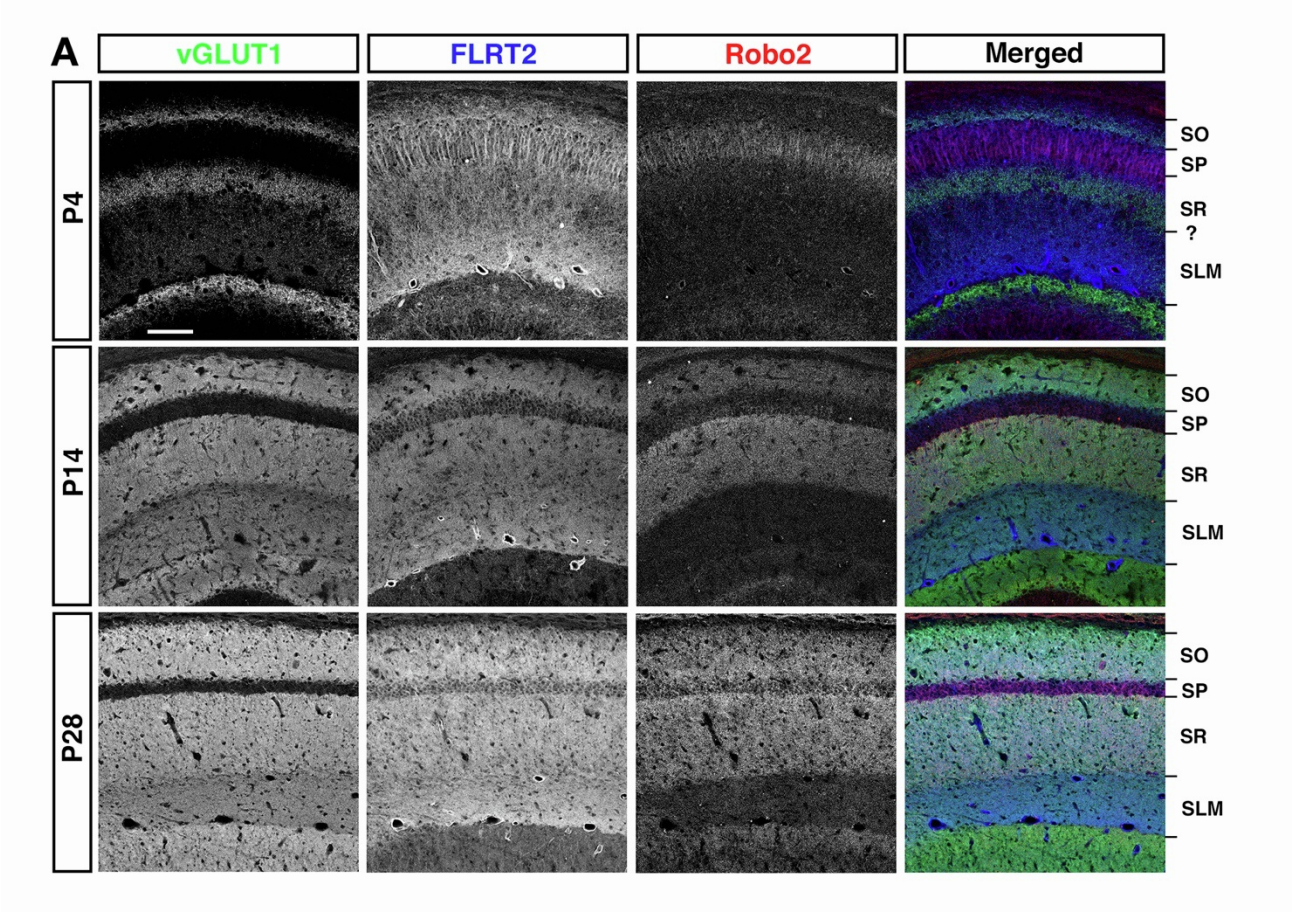

Figure S3 (related to Figure 2)

(**A**) Immunostaining for Robo2, FLRT2 and Vglut1 in hippocampal CA1 at three postnatal time points (P4, P14, P28). At P4, Robo2 expression is restricted to the pyramidal layer and proximal dendrites. By P14, Robo2 enrichment in SO and SR layers (but exclusion from SLM) observed at P28 is already visible. Note that Vglut1 expression, indicating the presence of excitatory presynaptic axons is also restricted to thin stripes in SO and very proximal SR suggesting that innervation of CA1 PNs starts in most proximal portions of their dendritic arbor. Interestingly, at all three ages, FLRT2 protein localization is observed in all sublayers of CA1.

Scale bar: 50µm

A

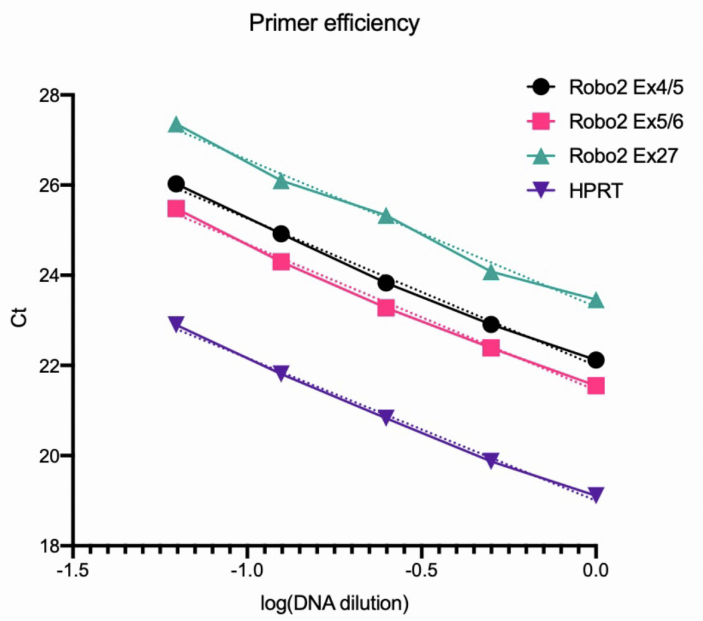

	Forward	Reverse
Robo2 Ex4/5	AGAGCTCACTGTCTTTGAACG	GGGATCTCCTTGGACCTGAC
Robo2 Ex5/6	GCCAACGGTGAGGTGGAAAA	AACTGTGGAGGAGCAACAGG
Robo2 Ex27/28	AGCAGCCAACTTAGAAGACACA	CACCAGGGACTCCTCTGATCC
HPRT	AGCAGGTGTTCTAGTCCTGTGG	ACGCAGCAACTGACATTTCTAA

	Slope	Efficiency (%)	R^2
Robo2 Ex4/5	-3.27	102.41	0.99
Robo2 Ex5/6	-3.24	103.36	1.00
Robo2 Ex27/28	-3.26	102.56	0.99
HPRT	-3.16	107.19	1.00

B

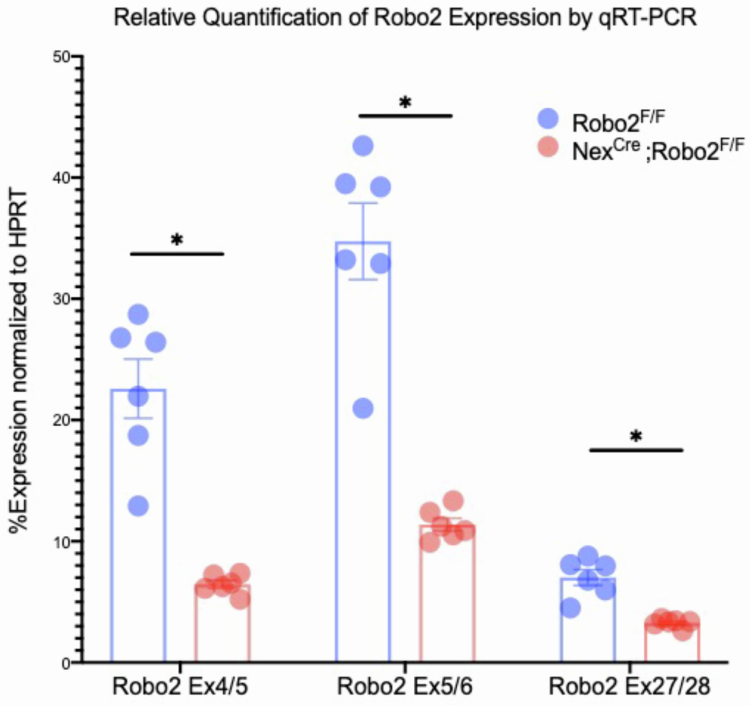

Figure S4 (related to Figures 2 and 4).
(**A**) Linear regression of Cycle threshold (Ct) as a function of log(DNA dilution) of corresponding cDNA from the hippocampus showing linear amplification of the designed primers for the quantitative RT-PCR (qRT-PCR). Tables provides sequences of the primers as well as the slope, amplification efficiency (%)

and R-squared values of each couple of PCR primers. Exons spanned by the corresponding primer sets were designed using NCBI Primer-BLAST tool.

(**B**) Summary of the qRT-PCR of *Robo2* mRNA expression in dissected hippocampi isolated from adult $Robo2^{F/F}$ and Nex^{Cre};$Robo2^{F/F}$ mice (n= 6 mice per condition, unpaired non-parametric t-test -- Mann-Whitney -- with a p-value threshold at 0.05). qRT-PCR of HPRT mRNA was used as internal control.

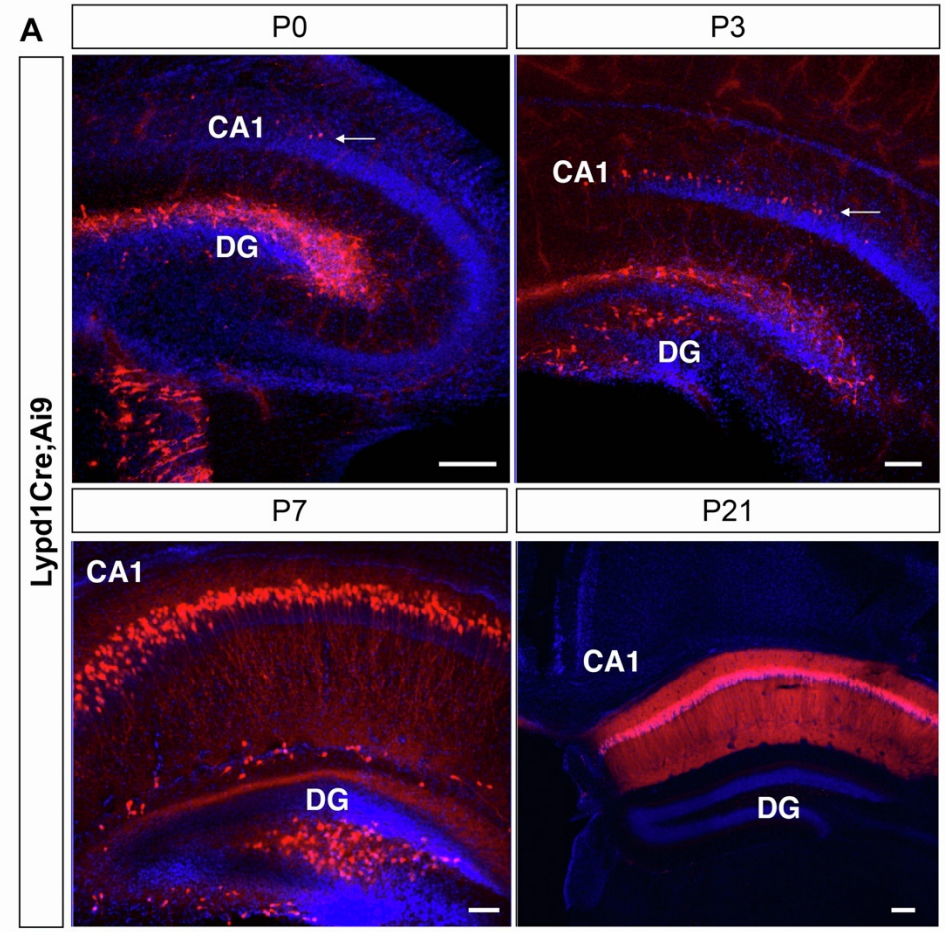
A
P0
P3
P7
P21
Lypd1Cre;Ai9
CA1
DG
CA1
DG
CA1
DG
CA1
DG

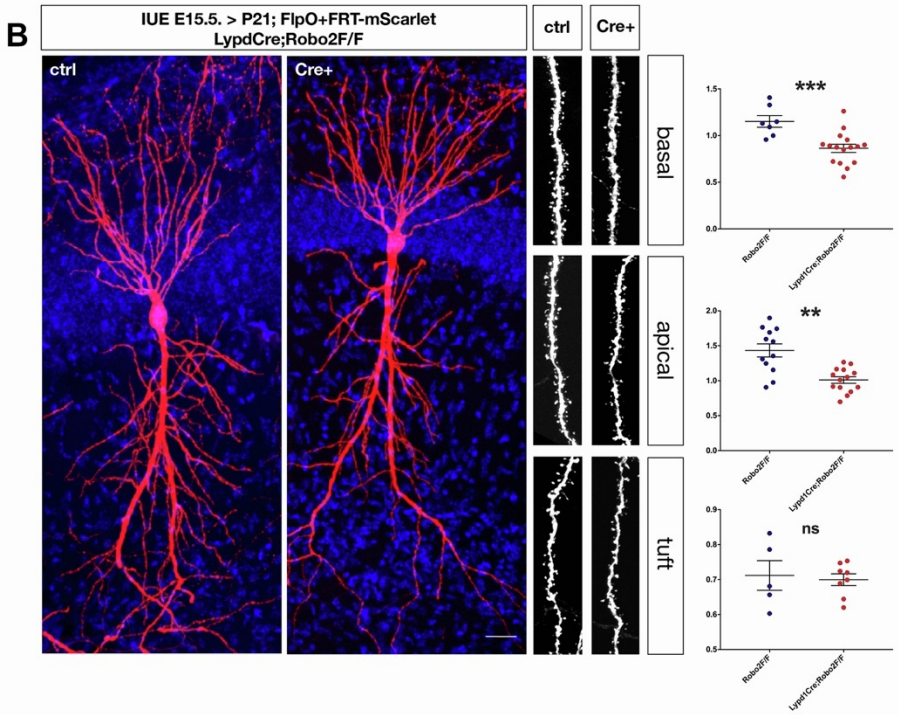
B
IUE E15.5. > P21; FlpO+FRT-mScarlet
LypdCre;Robo2F/F
ctrl
Cre+
ctrl
Cre+
basal
apical
tuft
***
**
ns
Robo2F/F
Lypd1Cre;Robo2F/F

62

Figure S5 (related to Figure 2)

(**A**) Analysis of onset of Cre-expression in Lypd1^{Cre};Ai9 mice. The Ai9 reporter mouse line expresses tdTomato upon Cre-dependent recombination of a LoxP-STOP-LoxP cassette. Histological analysis of Ai9 expression following recombination by the Lypd1^{Cre} driver line at P0, P3, P7 and P21. Expression is sparse at P0 and P3 and increases over the first postnatal week to peak at P7 and clearly CA1 PNs specific by P21. Scale bars: 150µm, 75µm, 50µm, 50µm.

(**B**) Spine density is decreased in SO and SR dendritic domains of Lypd1^{Cre};Robo2$^{F/F}$ CA1 PNs compared to control (Robo2$^{F/F}$ only). Hippocampal *in utero* co-electroporation of a pCAG:FlpO and a pCAG:Frt-STOP-Frt::mScarlet1 was performed into Lypd1^{Cre};Robo2F/F and Robo2$^{F/F}$ control littermates in order to achieve FlpO-dependent sparse expression of mScarlet (red) in CA1 PNs of both genotype. Analysis of spine density shows a decrease in proximal dendritic compartments in Robo2 KO CA1 PNs, akin to the sparse HIUE approach shown in Figure 2.

Scale bar: 40µm. Number of segments analyzed from at least 3 adult mice: basal (SO): Robo2$^{F/F}$ n=7 (mean=1.152, SD+/-0.16), Lypd1^{Cre};Robo2$^{F/F}$ n=16 (mean=0.863, SD+/-0.17), p=0.0005; apical oblique (SR): Robo2$^{F/F}$ n=12 (mean=1.433, SD+/-0.32), Lypd1^{Cre};Robo2$^{F/F}$ n=14 (mean=1.011, SD+/-0.17), p=0.011; apical tuft (SLM): Robo2$^{F/F}$ n=5 (mean=0.711, SD+/-0.09), Lypd1^{Cre};Robo2$^{F/F}$ n=8 (mean= 0.697, SD+/-0.047), p>0.99 using a Mann-Whitney non-parametric test.

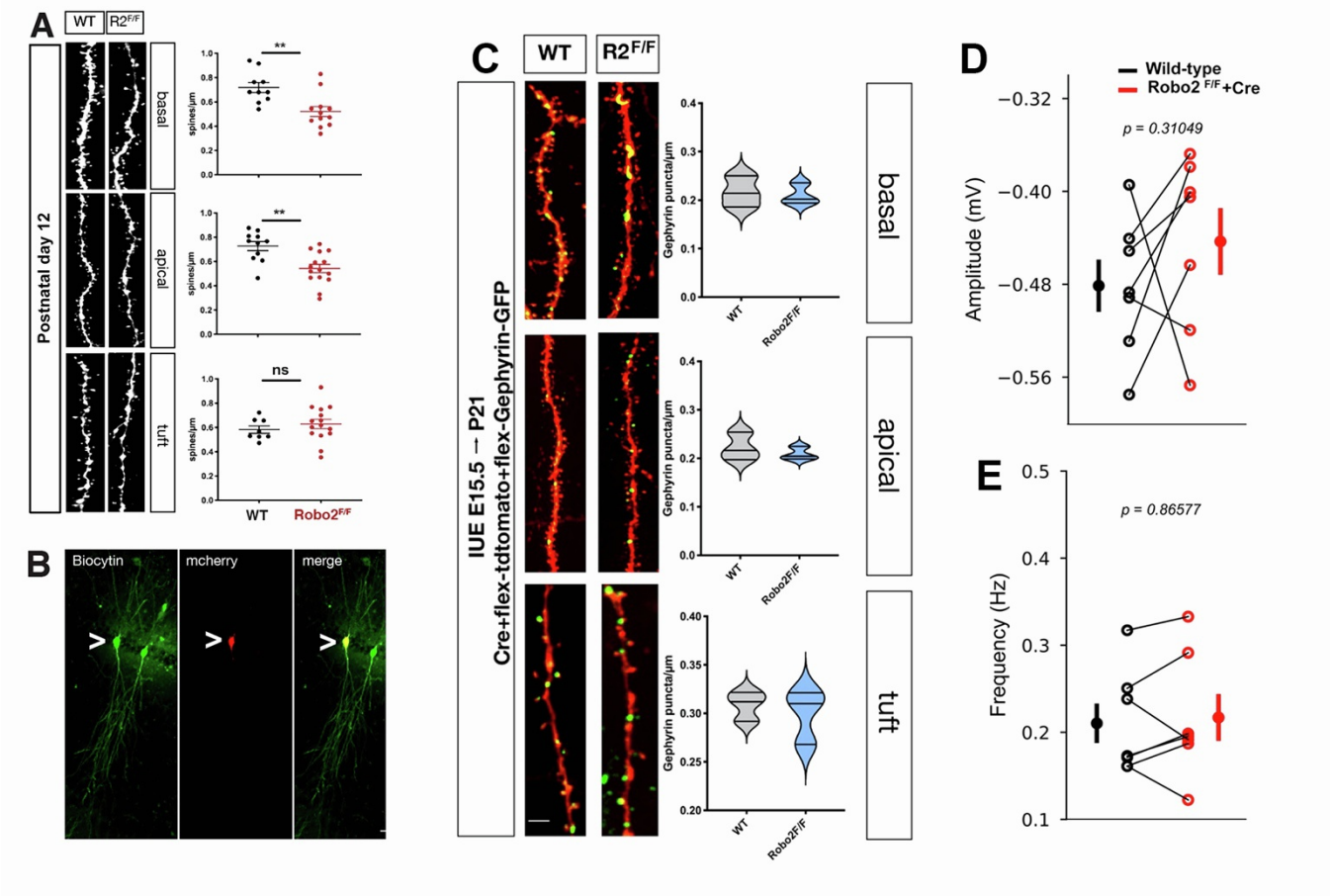

Figure S6 (related to Figure 2)

(**A**) Robo2 is required for synaptic development, rather than maintenance. Spine analysis of P12 wild-type or Robo2$^{F/F}$ CA1 PNs electroporated with Cre + FLEX::tdTomato shows a similar phenotype seen at P21 is already present at the peak of synaptogenesis. Representative images of dendritic branch segments. (basal: WT: n=10 dendritic segments, mean=0.72 spines/µm +/-0.037 (SEM), KO: n=12 dendritic segments, mean=0.52 spines/µm +/-0.034 (SEM), reduction=27.41%, **p<0.01, Mann-Whitney; apical: WT: n=11 dendritic segments, mean=0.72 spines/µm +/-0.095 (SEM), KO: n=15 dendritic segments, mean=0.54 spines/µm +/-0.041 (SEM), reduction=22.35%, **p<0.01, Mann-Whitney), but not distal tuft dendrites (tuft: WT: n=8 dendritic segments, mean=0.58 spines/µm +/-0.031 (SEM), KO: n=15 dendritic segments, mean=0.63 spines/µm +/-0.037 (SEM), p=0.29, ns, Mann-Whitney). Scale bar: 10µm.

(**B**) Representative image of hippocampal slice used for electrophysiological recordings of EPSCs and IPSCs showing example of two adjacent CA1 PNs filled with biocytin (stained post-hoc with Streptavidin-488; green) to unambiguously identify that PNs recorded via patch-clamp were either control CA1 PNs (non-electroporated i.e. green only) or CA1 PNs previously *in utero* electroporated with mCherry and Cre (red with arrowhead). Scale bar: 20µm.

(**C**) Analysis of inhibitory synapse density in CA1 PNs. HIUE was used to induce sparse Cre-dependent expression of FLEX::EGFP-Gephyrin and FLEX::tdTomato into CA1 PNs during development. Density of gephyrin+ inhibitory synapses density at P21 is not significantly different between Robo2 KO and WT CA1 PNs. Scale bar: 15µm. Number of segments: basal: WT n=7 (mean=0.21, SD+/-0.03), $Robo2^{F/F}$ n=16 (mean=0.21, SD+/-0.02), p>0.99; apical: WT n=11 (mean=0.22, SD+/-0.03), $Robo2^{F/F}$ n=11 (mean=0.21, SD+/-0.01), p>0.99; tuft: WT n=6 (mean=0.31, SD+/-0.01), $Robo2^{F/F}$ n=8 (mean=0.29, SD+/-0.03), p=0.7. Mann-Whitney test.

(**D-E**) Analysis of mIPSPs in acute hippocampal slices. mIPSP analysis between P24-27 shows no difference in either frequency (WT: mean=0.205 Hz, SEM=0.027 Hz; KO: mean=0.201 Hz, SEM=0.028 Hz) or amplitude (WT: mean=-0.48 mV, SEM=0.023 mV; KO: -0.44 mV, SEM=0.029 mV) of miniature inhibitory synaptic events in Robo2 KO and WT CA1 PNs (paired recordings as in Figure 2). Data is from 7 pairs of WT and KO cells, p-values are indicated on the figure. Wilcoxon-signed rank test.

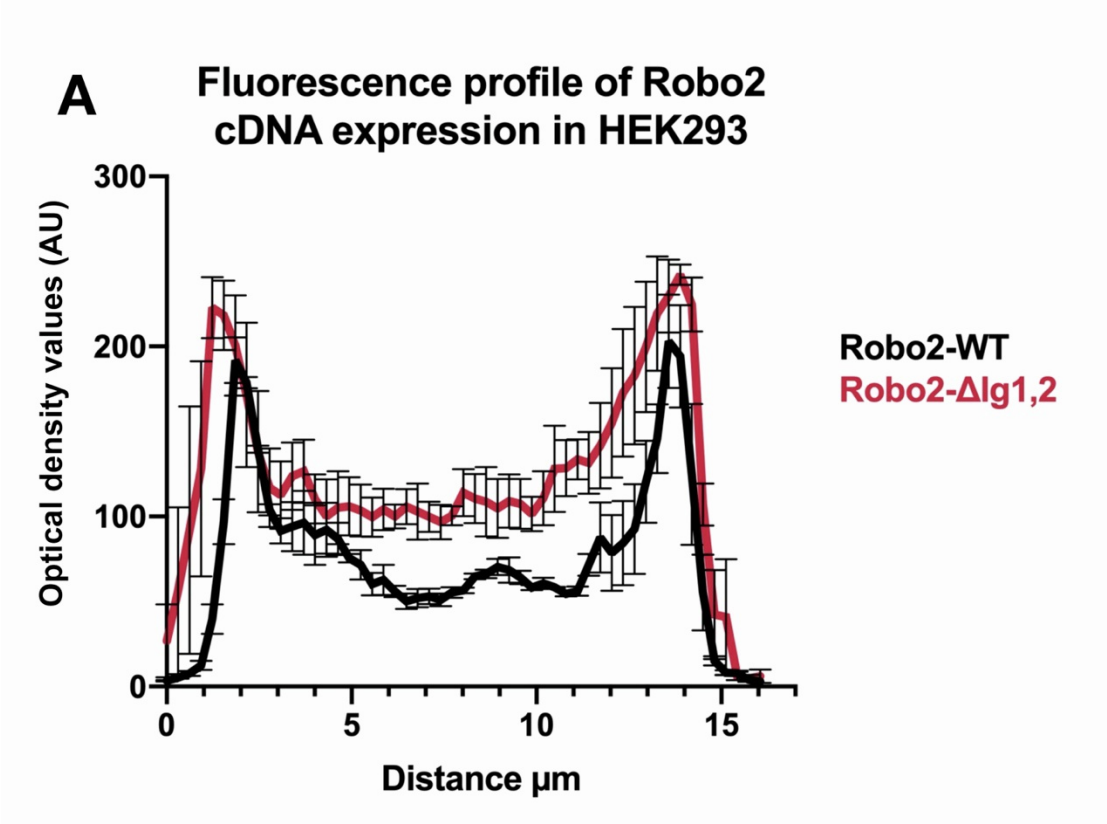

Figure S7. (related to Figure 3)

(**A**) Quantification of EGFP optical density showing membrane targeting of wild-type Robo2-EGFP and Robo2-ΔIg1,2-EGFP in HEK293 cells used in the synaptogenic co-culture assay (shown in Fig. 3). Line profile of optical density values for 12 different cells were averaged and plotted with cell diameter on the x-axis. Values represent mean of 3 biological replicates with >40 cells/replicate with SEM.

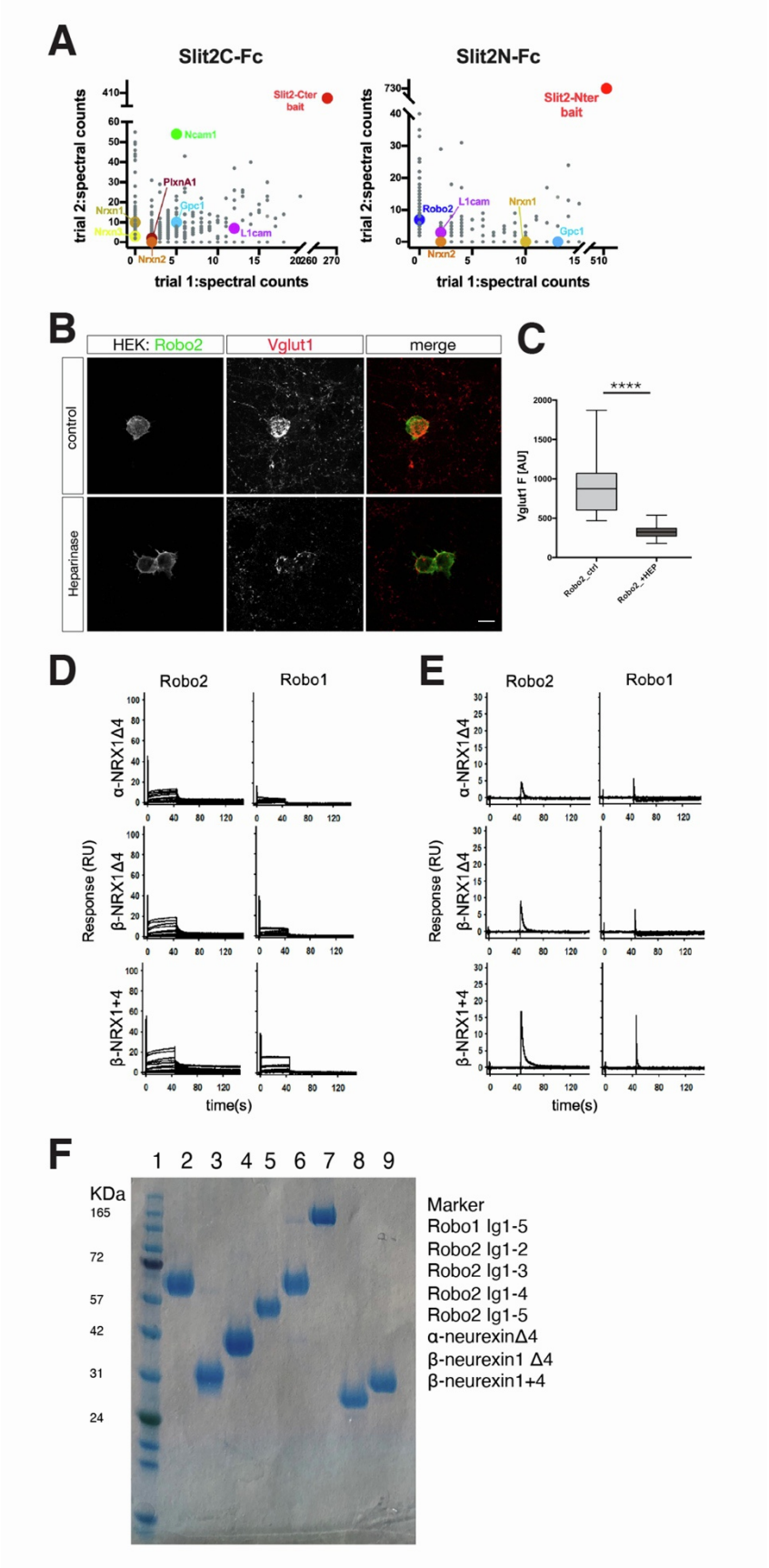
A
Slit2C-Fc
Slit2N-Fc
trial 2:spectral counts
trial 1:spectral counts
Slit2-Cter bait
Slit2-Nter bait
Ncam1
PlxnA1
Gpc1
L1cam
Nrxn1
Nrxn2
Robo2
B
HEK: Robo2
Vglut1
merge
control
Heparinase
C
****
Vglut1 F [AU]
Robo2_ctrl
Robo2_HEP
D
E
Robo2
Robo1
α-NRX1Δ4
β-NRX1Δ4
β-NRX1+4
Response (RU)
time(s)
F
1 2 3 4 5 6 7 8 9
KDa
165
72
57
42
31
24
Marker
Robo1 Ig1-5
Robo2 Ig1-2
Robo2 Ig1-3
Robo2 Ig1-4
Robo2 Ig1-5
α-neurexinΔ4
β-neurexin1 Δ4
β-neurexin1+4

118

Figure S8. (related to Figure 4)

(**A**) Mass-spectrometry results from synaptosome pulldown using SlitC-Fc and SlitN-Fc. Highlighted are cell surface adhesion proteins. Plotted data represents Ig-subtracted peptides only.

(**B**) Treatment of *in vitro* hemisynapse assay with Heparinase reduces Robo2-dependent Vglut1 clustering. Scale bar: 7µm.

(**C**) Quantification of data shown in Panel B. (****p<0.0001, Mann-Whitney).

(**D**, **E**) SPR binding experiments of Robos over Neurexins: Binding of Robo2 and Robo1 (Ig1-5) over surfaces immobilized with α-NRX1Δ4, β-NRX1Δ4, and β-NRX1+4 ectodomains. (D) Binding of Robos in the absence of heparin and (E) binding traces of Robos to Nrxns in the presence of 3mM EGTA (Ca^{2+} chelator), instead of 3mM $CaCl_2$.

(**F**) Coommassie blue stained gel showing quality and purity of all proteins used in SPR experiments.